Bulletin of the Seismological Society of America, Vol. 97, No. 1B, pp. 265–280, February 2007, doi: 10.1785/0120060100

Spatial Gradient Analysis for Linear Seismic Arrays

by Charles A. Langston

Abstract I incorporate the spatial gradient of the wave field recorded from one-dimensional arrays into a processing method that yields the horizontal-wave slowness and the change of geometrical spreading with distance. In general, the model for seismic-wave propagation is enough to be appropriate for body and surface waves propagating from nearby seismic sources but can be simplified into a plane-wave model. Although computation of the spatial gradient requires that array elements be closer than 10% of the horizontal wavelength, seismic-array apertures, in the usual sense, may extend over many horizontal wavelengths and illuminate changes within the wave field. Array images of horizontal slowness and the relative geometrical-spreading changes of seismic waves are derived using filter theory and used to interpret observed array wave fields. Errors in computing finite-difference spatial gradients from array nodes are explicitly considered to avoid spatial aliasing in the estimates. I apply the method to interpret waves in strong ground motion and small-scale refraction data sets. Use of the wave spatial gradient accentuates spatial differences in the wave field that can be theoretically exploited in fine-scale tomographic studies of structure and is complementary to frequency/wavenumber or beam-forming array-processing techniques.

Introduction

Many characteristics of observed seismic-wave fields can only be inferred by using dense arrays of seismic instruments. Indeed, most high-resolution active and passive seismic experiments require seismic arrays to collect enough data to either observe a characteristic wave-propagation effect, like horizontal-phase velocity, and to reduce the effects of secondary noise signals. Dense seismic arrays are the basis of the reflection and refraction techniques, and are also used to infer slowness and azimuth from natural and active source signals at large distances.

Most array analyses involve time-domain and frequency-domain methods to detect a signal sweeping across the array and then to measure its direction and velocity of propagation. Controlled experiments, such as the refraction method or reflection method, may simplify the array geometry by arranging seismic instruments in line from the source and assume simple wave-propagation models to derive attributes from the observed wave field that can be used to model Earth's medium or to image geological structure. The principal attribute of the seismic wave that is of interest is its spectral phase or time lag across the array with secondary consideration given to wave coherency to improve signal-to-noise ratios. The array is used to reduce a spatially complex wave field into a few component waves of interest. Of more fundamental importance to this article is the recognition that all array methods employ the same basic seismological field variable in the form of filtered ground displacement (and its time derivatives).

The basic thesis of this article is that spatial variation of the seismic wave field, loosely the strain or more exactly the displacement gradient, can reveal important wave attributes about individual seismic waves that can be used to infer medium properties and to identify those waves. Broadly speaking, the displacement gradient is more closely related to the mechanical properties of the medium through Hooke's law than is displacement itself and represents an alternative view of seismic-wave propagation through the wave equation. To motivate this idea with a basic theoretical example, consider a simple one-dimensional wave equation for a propagating shear wave in purely elastic media

$$\frac{\rho}{\mu}\frac{\partial^2 u}{\partial t^2} - \frac{\partial^2 u}{\partial x^2} = \left(\sqrt{\frac{\rho}{\mu}}\frac{\partial}{\partial t} - \frac{\partial}{\partial x}\right)\left(\sqrt{\frac{\rho}{\mu}}\frac{\partial}{\partial t} + \frac{\partial}{\partial x}\right) u = 0, \qquad (1)$$

where ρ is mass density and μ is the shear modulus. The usual scientific program in seismology is to make a measurement of u and of $V_s = \sqrt{\mu/\rho}$ to characterize the wave and to determine the medium properties. Although the field variable and the wave velocity may be easily measured, there is no guarantee that, even under ideal circumstances, equation (1) represents the correct physics of the wave propa-

gation. Unambiguous verification of equation (1) can only occur experimentally if $\partial^2 u/\partial t^2$, V_s, and $\partial^2 u/\partial x^2$ can be simultaneously measured and shown to be consistent. This suggests that another fruitful approach to experimental seismology could involve a measurement of the spatial dependence of u, a procedure that is rarely done.

Equation (1) is also factored into separate differential operators to emphasize that simple propagating waves of the form $u = f[t \pm (x/V_s)]$ can be considered separately and satisfy their own first-order differential equations (e.g., Whitham, 1999). The wave equation, in this simple example, requires a link between first-order time and spatial derivatives for elementary propagating waves.

The measurement of seismic wave-field displacement gradient and strain has, in general, been in the domain of the analysis of strong ground motion data from large earthquakes (e.g., Spudich *et al.*, 1995; Bodin *et al.*, 1997; Gomberg *et al.*, 1999) because strain and the coherency of strong ground motions are major issues in the design of large structures such as bridges and pipelines (Harichandran and Vanmarcke, 1986; Abrahamson, 1991; Zerva and Zervas, 2002). The motivation for this report comes from a recent analysis of strong-motion array observations from large explosions in unconsolidated sediments within the central United States (Langston *et al.*, 2006). It was shown that a very simple analysis of the displacement gradient along the linear array, assuming a plane-wave wave-propagation model, yielded surprisingly accurate estimates of the horizontal-phase velocity for seismic phases as a function of arrival time.

The purpose of this article is to expand the analysis of the seismic displacement gradient for linear seismic arrays using a generalized model of a seismic wave. This model includes geometrical spreading, spatially dependent wave slowness, and anelastic attenuation. The theory rests on the fundamental use of wave-amplitude observations to infer the basic characteristics of wave propagation that include the variation of wave amplitude with distance and horizontal-wave speed. Spatial gradient analysis is a seismic-wave-processing technique that is complementary to wavenumber spectral methods by directly addressing how seismic-wave amplitudes change with position. The method yields time-dependent maps of horizontal-phase velocity and amplitude variations that can be used to interpret and model the seismic-wave field.

This method may be useful for the analysis of a variety of seismological array experiments that include seismic refraction, surface-wave dispersion, seismic reflection, strong ground motion, acoustic, and regional/teleseismic arrays. The technique will be developed in detail for a linear array and applied to strong-motion and seismic-refraction data sets to show its strengths and weaknesses. The theory is expanded to two-dimensional arrays in a companion article (Langston, 2007) to show how it can be used for passive array deployments to analyze scattered wave fields and to determine time-varying array beams of seismic waves.

A Spatial Gradient Theory for One-Dimensional Arrays

A Wave with Geometrical Spreading and Distance-Dependent Slowness

The interpretation of array data almost always relies on the characteristics of a wave-propagation model. This is particularly true in frequency/wavenumber or beam-forming analyses, like slant stacking, where wave fields are assumed to be superpositions of plane waves. My fundamental assumption on the wave field involves a generalization of a single propagating wave from a point source to give flexibility in applying the technique where an array is situated very close to the source, as in reflection or refraction methods. The displacement, $u(t,x)$, of a simple refracted body wave or surface wave propagating in a medium with slowly varying physical properties can be represented by

$$u(t,x) = G(x)\, f(t - p(x - x_0)), \tag{2}$$

where, $G(x)$ is the geometrical spreading, p is the horizontal-wave slowness, and x_0 is a reference position. Here p is assumed to vary with distance x. This form of wave displacement naturally models individual body-wave rays in vertically inhomogeneous media and surface waves in media where the material property changes occur over scales greater than a wavelength. Differentiating equation (2) with respect to x gives

$$\frac{\partial u}{\partial x} = A(x)u + B(x)\,\frac{\partial u}{\partial t}, \tag{3}$$

where

$$A(x) = \frac{G'(x)}{G(x)} \tag{4}$$

and

$$B(x) = \frac{\partial}{\partial x}\left[-p(x - x_0)\right] = -\left[p + \frac{\partial p}{\partial x}\,(x - x_0)\right]. \tag{5}$$

Equation (3) represents a relationship between three different time series: the spatial derivative of wave displacement, wave displacement, and wave particle velocity through the coefficients $A(x)$ and $B(x)$. The coefficients themselves contain important information about the wave. Integrating $A(x)$ over the interval $[x_0, x]$ gives the geometrical spreading:

$$\int_{x_0}^{x} A(x)dx = \ln\frac{G(x)}{G(x_0)}. \tag{6}$$

Integrating $B(x)$ over the same interval gives the horizontal-wave slowness:

$$p = -\frac{1}{(x - x_0)} \int_{x_0}^{x} B(x)dx. \tag{7}$$

Note that the limit of equation (7) as $x \rightarrow x_0$ is $-B(x_0)$, or $p(x_0)$, using L'Hospital's rule. Thus, observations of displacement gradient, displacement, and velocity at a single location could be used through equation (3) to derive a point measurement of geometrical spreading and wave slowness. Application of equation (3) over a linear array would yield the variation of both geometrical spreading and horizontal slowness with position that could then be used as data in an inversion for earth structure.

It is useful at this point to give three examples of waves that can be represented by equation (2). First, consider a plane wave propagating in the $+x$ direction. In this case $G(x) =$ constant and p is constant. The relationship between the displacement gradient and velocity is just

$$\frac{\partial u}{\partial x} = -p \frac{\partial u}{\partial t}. \tag{8}$$

This relation was used in Langston *et al.* (2006) to find time-dependent phase velocity for strong-motion body and surface waves.

A Rayleigh or Love wave at a single period in non-attenuating media has a geometrical spreading of $G(x) = x^{-1/2}$ and a constant horizontal slowness, p. The relationship equation (3) is

$$\frac{\partial u}{\partial x} = -\frac{1}{2x} u - p \frac{\partial u}{\partial t}. \tag{9}$$

In this case $f(t)$ will be a monochromatic time series with the period of the surface wave.

A single refracted body wave in vertically inhomogeneous media has a geometrical spreading related to the details of the velocity gradient at the turning point and a change in horizontal slowness (or ray parameter) with distance also related to the velocity model (i.e., $p = p(x)$). In this case the general equation (3) is the operating relationship. If the geometrical spreading can be represented by $G(x) = x^{-n}$, then

$$\frac{\partial u}{\partial x} = -\frac{n}{x} u - \left[p + \frac{\partial p}{\partial x} (x - x_0)\right] \frac{\partial u}{\partial t}. \tag{10}$$

My expectation in applying the assumptions of equation (2) to data is that an observed seismogram will be the superposition of many different waves occurring sequentially in time. There is no guarantee that this assumption will be true for any particular time window, because it is obvious that two or more waves could interact at the same time. If two waves are separated in time or have significantly different frequency content but arrive at the same time, then I will show that equation (2) can directly apply to their study. Equation (2) is not appropriate for time interference of waves with similar frequency content. However, this will be discussed in the following.

Solving for $A(x)$ and $B(x)$ in equation (3) could be done in a variety of ways, assuming that the three time series for displacement gradient, displacement, and velocity are available. Equation (3) could be solved in either the time or frequency domain by discretely sampling the time or frequency series and setting up a typical least-squares problem. For example, in the time domain for a particular position x, a system of equations can be set up

$$\underset{\sim}{G}\,\underset{\sim}{m} = \underset{\sim}{d} \tag{11}$$

where,

$$\underset{\sim}{G} = \begin{bmatrix} u(t_0, x) & u_{,t}(t_0, x) \\ u(t_1, x) & u_{,t}(t_1, x) \\ & \vdots \\ u(t_m, x) & u_{,t}(t_m, x) \end{bmatrix}, \tag{12}$$

$$\underset{\sim}{m} = \begin{bmatrix} A(x) \\ B(x) \end{bmatrix}, \tag{13}$$

and

$$\underset{\sim}{d} = \begin{bmatrix} u_{,x}\,(t_0, x) \\ u_{,x}\,(t_1, x) \\ \vdots \\ u_{,x}\,(t_m, x) \end{bmatrix}, \tag{14}$$

with the comma subscript notation denoting differentiation with respect to x or t. This system of equations is overdetermined, in general, for more than one independent time (or frequency) sample of the time series and can be solved using standard linear inversion methods.

Alternatively, $A(x)$ and $B(x)$ may be found quickly from equation (3) using Fourier transforms and filter theory. Fourier transforming equation (3) gives

$$\hat{u}_{,x} = A(x)\hat{u} + B(x)\, i\omega\hat{u}. \tag{15}$$

Thus,

$$\frac{\hat{u}_{,x}}{\hat{u}} = A(x) + i\omega B(x) \tag{16}$$

giving

$$A(x) = \mathrm{Re}\left\{\frac{\hat{u}_{,x}}{\hat{u}}\right\} \tag{17}$$

and

$$B(x) = \frac{1}{\omega} \operatorname{Im}\left\{\frac{\hat{u}_{,x}}{\hat{u}}\right\}. \quad (18)$$

This method is particularly suited for a fast data-processing implementation involving the fast Fourier transform of a moving time window over the time series data.

Filtering

Because equation (3) is a linear equation, we are not restricted to exact forms of the displacement field variable. Every seismogram contains an instrument response and/or may be subsequently filtered to remove unwanted noise or interfering signals. Thus, equation (3) may be convolved with an operator that represents the recording system or specialized filter to be used in data processing. It should be obvious that filtering can be used to separate simultaneously arriving signals if the spectra of those signals do not overlap.

Of special interest to later data-processing schemes is a distance-dependent time shift due to a reducing velocity applied to the data. Suppose that a time shift due to a reducing velocity, v_r, is applied to every observation in a linear array. This can be represented by convolution with an impulse function so that the reduced displacement is

$$u_r(t, x) = u(t, x) * \delta\left(t + \frac{(x - x_0)}{v_r}\right) \quad (19)$$

giving

$$\frac{\partial u_r}{\partial x} = A(x)u_r + B_r(x)\frac{\partial u_r}{\partial t}. \quad (20)$$

The coefficient $B_r(x)$ is similar to equation (5) but now contains the reduced horizontal slowness, p_r:

$$B_r(x) = -\left[p_r + \frac{\partial p_r}{\partial x}(x - x_0)\right], \quad (21)$$

where

$$p_r = p - \frac{1}{v_r}. \quad (22)$$

Note that in a plane wave ($G(x) =$ constant and constant p), if a reducing velocity is chosen such that $p_r = 0$, then $A(x)$, $B_r(x)$, and $\partial u_r/\partial x$ are all zero. If a reducing velocity is applied to waves with geometrical spreading and constant slowness such that $p_r = 0$, then the displacement gradient is a consequence entirely of the geometrical spreading. The use of a constant reducing velocity will be an important requirement for being able to compute the displacement gradient from aliased array data (see below).

The Displacement Gradient, Noise, and Simultaneous Arrivals

Computation of the displacement gradient is a source of noise in this technique. The Appendix gives details on errors caused by the finite-difference approximation and ways of filtering the data to minimize these errors.

Although the finite-difference-error analysis serves as a guide for determining what wave numbers are appropriate for an array, there is the potential for larger, uncontrollable errors to creep in from seismic-instrument miscalibration or amplitude statics problems induced by geological structure or instrument installation.

It is straightforward to show that the error in the finite difference is directly proportional to the error in amplitude between seismometers.

The responses of modern seismometers are usually known to better than a few percent (Gomberg *et al.*, 1988) so that a well-calibrated group of instruments composing an array should introduce only small errors into the displacement gradient calculation. On the other hand, the near-surface is not a clear window into deeper structure of the earth (Cranswick *et al.*, 1985). It is well known that heterogeneity degrades the response of an array due to near-site focusing and defocusing of seismic waves (Bungum *et al.*, 1971). My analysis ideally uses a dense array to be able to sample the wave field well within one horizontal wavelength but it will also be subject to small-scale heterogeneity.

Even considering these problems, there is an additional problem on the nature of ground-motion noise. By definition, data from a gradiometer array is low-pass filtered to yield ground motions that are 10% or less of the horizontal wavelength of the array. It is very likely that noise signals will also be highly correlated across the array. It is not likely that the signal-to-noise ratio can be improved by denser spatial recording, but it might be improved by stacking multiple sources that occur at different times. Thus, the effect of correlated wave noise will be a function of the signal-to-noise ratio and essentially be the same problem as the interference of two (or more) waves.

Here is a simplified analysis of the problem. Suppose there are two waves $u(t)$ and $v(t)$, arriving at the same sensor at the same time. By superposition and using relation (15)

$$w_{,x} = u_{,x} + v_{,x} = A_1u + A_2v + B_1u_{,t} + B_2v_{,t} \quad (23)$$

where

$$w = u + v. \quad (24)$$

Fourier transform equation (23), divide through by the Fourier transform of w, and obtain the relations for the gradiometry coefficients (equations 17 and 18) for the total displacement:

$$A = \mathrm{Re}\,\frac{\hat{w}_{,x}}{\hat{w}} = A_1\,\mathrm{Re}\,\frac{\hat{u}}{\hat{w}} + A_2\,\mathrm{Re}\,\frac{\hat{v}}{\hat{w}} - \omega B_1\,\mathrm{Im}\,\frac{\hat{u}}{\hat{w}} - \omega B_2\,\mathrm{Im}\,\frac{\hat{v}}{\hat{w}} \quad (25)$$

$$B = \frac{1}{\omega}\,\mathrm{Im}\frac{\hat{w}_{,x}}{\hat{w}} = A_1\,\frac{1}{\omega}\,\mathrm{Im}\,\frac{\hat{u}}{\hat{w}} + A_2\,\frac{1}{\omega}\,\mathrm{Im}\,\frac{\hat{v}}{\hat{w}} - B_1\,\mathrm{Re}\,\frac{\hat{u}}{\hat{w}} - B_2\,\mathrm{Re}\,\frac{\hat{v}}{\hat{w}}. \quad (26)$$

Assume that the two waves have the same complex spectra differing only by horizontal-phase velocities p_1 and p_2, and amplitude a and b:

$$\begin{aligned}\hat{u}(\omega) &= a\hat{c}(\omega)e^{-i\omega p_1(x-x_0)}\\ \hat{v}(\omega) &= b\hat{c}(\omega)e^{-i\omega p_2(x-x_0)}\end{aligned} \quad (27)$$

v will be considered the source of noise in the signal so that $a > b$. The spectral ratios are given by

$$\frac{\hat{u}}{\hat{w}} = \frac{1 + \frac{b}{a}\,e^{+i\omega(p_2-p_1)(x-x_0)}}{1 + \frac{b^2}{a^2} + 2\,\frac{b}{a}\cos\,\omega\,(p_2 - p_1)(x - x_0)}$$

$$\frac{\hat{v}}{\hat{w}} = \frac{\frac{b^2}{a^2} + \frac{b}{a}\,e^{+i\omega(p_2-p_1)(x-x_0)}}{1 + \frac{b^2}{a^2} + 2\,\frac{b}{a}\cos\,\omega\,(p_2 - p_1)(x - x_0)}. \quad (28)$$

Since the waves are at the same position, let $x = x_0$, and for small b

$$\frac{\hat{u}}{\hat{w}} \simeq 1$$

$$\frac{\hat{v}}{\hat{w}} \simeq \frac{b}{a}. \quad (29)$$

This gives

$$A \simeq A_1 + A_2\,\frac{b}{a} = A_1 + A_2\,\mathrm{SNR}^{-1}$$

$$B \simeq B_1 + B_2\,\frac{b}{a} = B_1 + B_2\,\mathrm{SNR}^{-1}. \quad (30)$$

The error in the coefficients is proportional to the coefficients of the noise wave and inversely proportional to the signal-to-noise ratio (SNR). This shows that there are no major instabilities in the determination of the gradiometry coefficients due to simultaneously arriving waves with the same frequency content as long as one is relatively small. Of course, if two, equally large waves are interfering in the signal, it may be possible that a fictitious result or no result at all could be obtained in the analysis for that particular time and position. Collection of data at other positions along an array would be key in observing the moveout between the two phases. Treatment of the spectral ratio so it remains true to the basic assumption that $A(x)$ and $B(x)$ are constant is a key condition in making the array analysis function and is discussed next.

Processing Data from Linear Arrays

A Synthetic Example Using Filter Theory

Consider a wave model of the form

$$u(t, x) = \frac{e^{-100(t-1)^2}}{x} * \delta(t - px), \quad (31)$$

with $x = 2.55$ km and $p = 1/2.5$ sec/km. Anticipating the discussion of the strong-motion array in the following, I also assume a $\Delta x = 0.015$ km (15 m) for the finite-difference computation of the displacement derivative. The first issue is to produce an unaliased estimate of the displacement derivative (see Appendix). Equation (A3) can be recast into one of maximum allowable frequency, $f_{\max}$, as a function of horizontal-phase velocity, c, and Δx by specifying a maximum error threshold, δ. Here we set $\delta = 0.1$ to obtain

$$f_{\max} = \frac{c\sqrt{0.15}}{\pi\Delta x}. \quad (32)$$

The displacement derivative requires knowledge of both frequency and horizontal-phase velocity to choose the appropriate signal bandwidth for analysis. The maximum frequency is 20 Hz for the assumed horizontal phase velocity of 2.5 km/sec. As a practical matter, the analysis must proceed by first estimating the approximate slowness of observed signals and then using a relation like equation (32) to estimate the maximum allowable signal frequency for low-pass filtering before computing the displacement derivative. This avoids the spatial-aliasing effect pointed out by Lomnitz (1997) that occurs in strainmeters. In the case of our example wave, nearly all of the energy of the wave occurs at below 10 Hz (Fig. 1).

The second issue in applying the filter technique is estimating the errors in the coefficients $A(x)$ and $B(x)$. Perturbing the coefficients in equation (16):

$$(A + \delta A) + i\omega(B + \delta B) = \frac{\hat{u}_{,x} + \delta\hat{u}_{,x}}{\hat{u}} \quad (33)$$

and using equation (A3) as the estimate for $\delta\hat{u}_{,x}$ gives

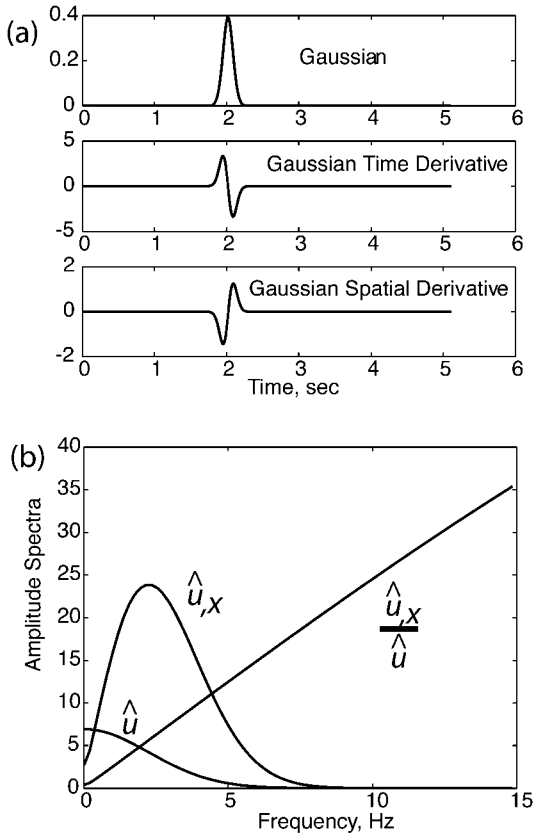

Figure 1. Synthetic example of spatial gradient analysis. (a) Shown are the assumed gaussian functional displacement (equation 31) for a propagating wave, its time derivative, and the spatial derivative computed by using the finite-difference method discussed in the text. (b) Displayed are the amplitude spectra of the displacement, $\hat{u}$, the spatial derivative, $\hat{u}_{,x}$, and the spectral ratio.

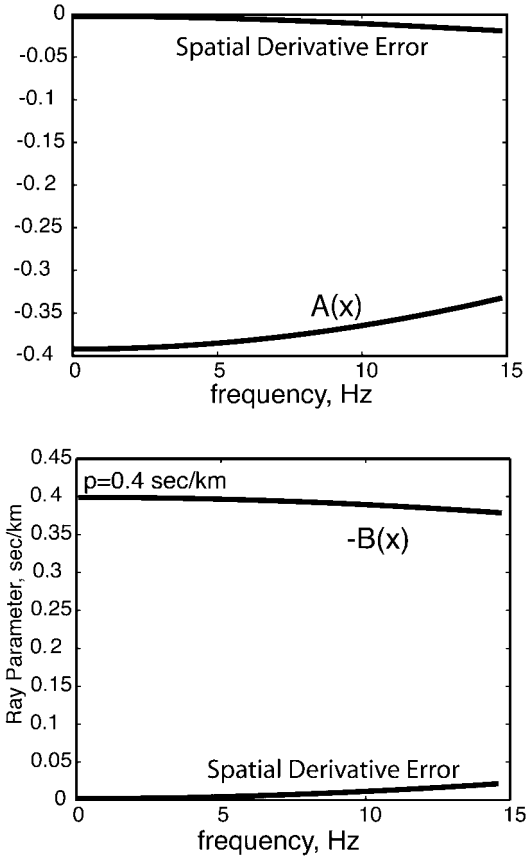

Figure 2. The coefficients $A(x)$ and $-\mathrm{B}(x)$ determined from equations (17) and (18) for the synthetic wave forms shown in Figure 1 as a function of frequency. Also shown in each panel is the spatial derivative error for the second-order finite difference (equation A3), assuming only a propagating plane wave. The values of the coefficients are exact at zero frequency but diverge according to that expected from the finite-difference error.

$$\delta A = \mathrm{Re}\left\{\frac{\delta \hat{u}_{,x}}{\hat{u}}\right\}$$
$$\delta B = \frac{1}{\omega}\,\mathrm{Im}\left\{\frac{\delta \hat{u}_{,x}}{\hat{u}}\right\}. \quad (34)$$

Figures 1 and 2 show the application of these relations. Error only occurs in the spatial derivative and is reasonably modeled by the finite-difference error analysis that assumes a simple plane wave. The errors in the geometrical spreading and slowness coefficients smoothly increase with frequency in a predictable way.

Example Using Strong-Motion Array Data

The test of method lies in how it works with a real field data set. Langston *et al.* (2006) used a simple forward difference to compute spatial displacement derivatives and equation (8) to analyze time series envelopes for horizontal slowness. The data consisted of three-component strong-motion accelerations (corrected to displacement) collected from a linear array of eight stations with 15-m spacing at distances of 1.3 and 2.5 km from two large explosions in the Mississippi embayment. The resulting slowness values for the larger amplitude seismic phases agreed quite well with estimates made by modeling phase arrival times across the array.

The data showed a variety of early-arriving high-frequency body waves and later-arriving lower-frequency surface waves (Fig. 3). There are a number of distinct phase arrivals but the seismograms generally show many phases grading into and interfering with each other.

The approach adopted here is to perform a moving-window analysis on the displacement gradient and displacement seismograms and apply equations (17) and (18) for the spectra in each time window. If there are coherent propagating phases within the seismogram, this strategy should be able to detect them and localize them in time. To avoid aliasing in the spatial derivative, the horizontal slowness of target sections of filtered seismograms is estimated by graph-

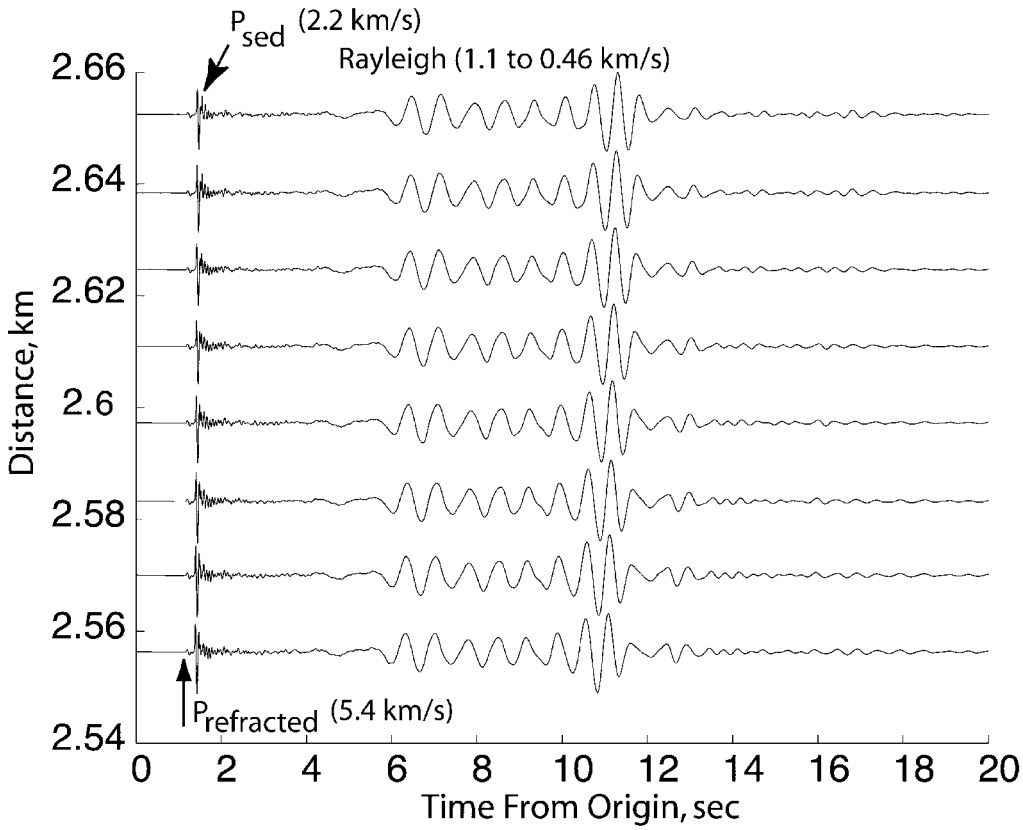

Figure 3. Vertical-component strong-motion data collected from a large explosion in the Mississippi embayment (Langston *et al.*, 2006). The data have been corrected to displacement and show a highly coherent refracted P wave, $P_{\text{refracted}}$, the P wave trapped in the unconsolidated sediments of the Mississippi embayment, P_{sed}, and a lower-frequency Rayleigh wave train. Also shown are measured horizontal-phase velocities measured in the previous study.

ically looking at phase moveout across the array. This sets the maximum frequency for a two-pole phaseless Butterworth bandpass filter using relation (32). Another approach could be to compute the frequency-wave number spectra for just the displacement field to estimate wave number and frequency bands appropriate to the data. The minimum frequency for the bandpass filter will usually depend on the signal-to-noise ratio, instrument passband, or simply a choice based on the characteristics of the signal. The data are windowed in the time domain through multiplication with a boxcar of unit height with 10% cosine tapers at both ends. The width of the window is predefined as and shifted along the time series by one eighth of its width.

Real seismic signals will also be subject to various sources of noise. In particular, the spectral ratios in equations (17) and (18) may be ill-behaved because of spectral nulls in the displacement spectra or the interference of other propagating waves with the phase of interest. Remember that equations (17) and (18) require that $A(x)$ and $B(x)$ be constant over the analysis frequency band. There is nothing to guarantee that the coefficients be constant in real data because this is simply an assumption of the analysis. Analysis of the strong-motion data set immediately reveals this problem with spectral ratios but also suggests a solution for practical data analysis. Figure 4 shows the result for the spatial gradient wave field evaluated at sensor 2 of the explosion data set. The P wave is highly coherent across the array in this frequency band and shows a very simple pulselike form. Both the $A(x)$ coefficient and $B(x)$ coefficient results show large fluctuations. Arrival times with large variations in the coefficients are also associated with large variance in the real and imaginary parts of the spectral ratio. These occur before the major P-wave arrivals and reflect the background noise field and after the P wave arrival in the P-wave coda. If the coefficients are filtered by only showing those estimates that are better than twice the standard deviation of the estimate, then the analysis yields appropriate horizontal-phase velocities for the refracted and reflected P waves in the signal (Fig. 5). Both waves speed up somewhat near the center of the array. This might suggest a small amplification effect in site response at the fourth array sensor. However, the $A(x)$ coefficient becomes more negative for this sensor as shown in Figure 6. The phase velocity and relative change in geometrical spreading is proportional to an amplitude ratio

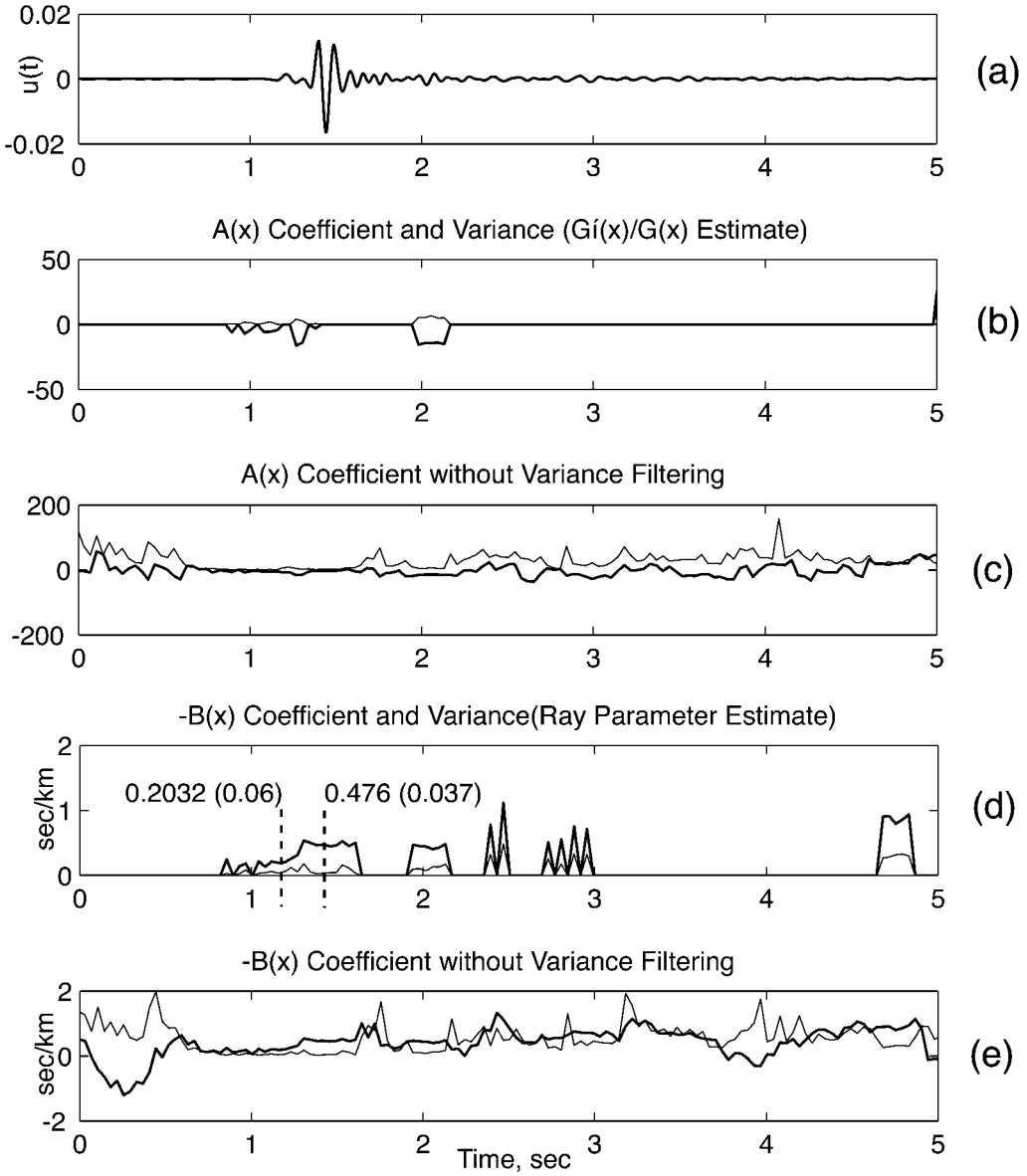

Figure 4. Example of processing the *P*-wave data for the second station (near 2.57 km; Fig. 3) using spatial gradient analysis. A two-pole, phaseless bandpass Butterworth filter with corner frequencies of 10 and 15 Hz was used to filter the data before taking the spatial gradient. The spatial gradient was computed using the data for the first and third station, and the moving time window analysis used a time window width of 0.3 sec. (a) shown are the filtered displacement data at station 2. (b) shown are the value of the $A(x)$ coefficient, determined as the mean of the spectral ratio, as a function of time after using variance filtering as discussed in the text. Those values of $A(x)$ are kept if they are greater than twice the standard deviation of the spectral ratio. The heavy line shows the coefficient and the thin line shows the standard deviation of the spectral ratio. (c) Shown are the $A(x)$ coefficient and standard deviation for the entire processed time series. Note that much of the signal has a standard deviation much larger than the mean. (d) Shown is a similar plot for the $-B(x)$ coefficient after variance filtering. The horizontal slowness of $P_{\text{refracted}}$ and P_{sed} is 0.2032 $\pm$ 0.06 sec/km and 0.476 $\pm$ 0.037 sec/km, respectively. This translates into 3.8 to 6.9 km/sec and 1.94 to 2.28 km/sec horizontal-phase velocity, respectively. (e) Shown is the $-B(x)$ coefficient and its standard deviation for the entire time series.

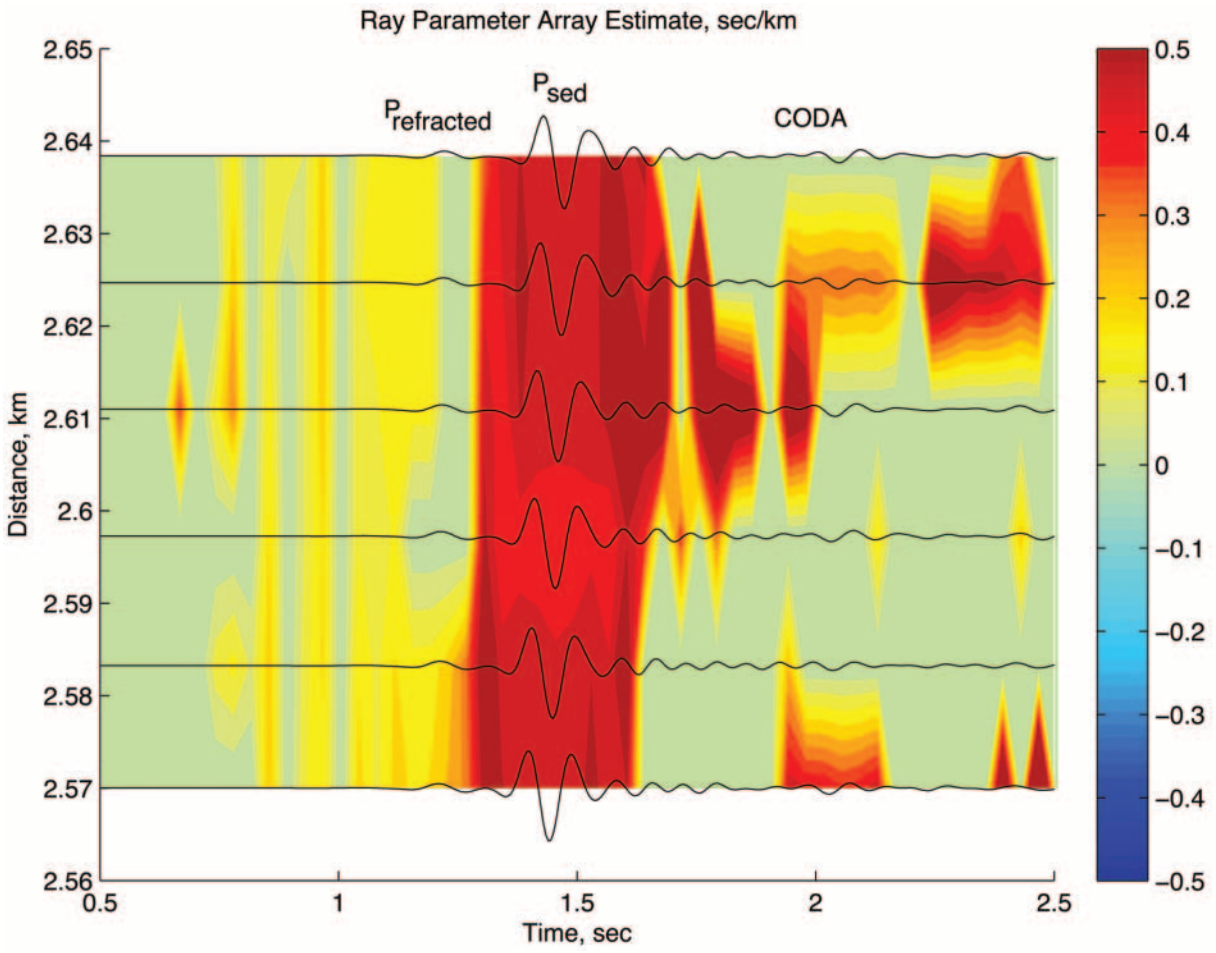

Figure 5. Colored contour plot showing the ray parameter estimate (from $-B(x)$) for the central six elements of the strong-motion array. The estimates appear to be relatively stable for both $P_{\text{refracted}}$ and P_{sed}. Relatively slow-moving waves appear erratically in the coda.

(equations 17 and 18). If the denominator becomes larger, then the slowness will become smaller (faster horizontal velocity) but the change in geometrical spreading also becomes smaller. These effects of site amplification (or deamplification) should be kept in mind while interpreting images of the wave coefficients.

The algorithm was applied in the frequency band from 1 to 3 Hz to examine the characteristics of vertical Rayleigh waves propagating across the array (Figs. 7 and 8). The vertical Rayleigh wave train starts at about 5 sec arrival time with higher-mode waves traveling at 1 km/sec to 0.75 km/sec (1 sec/km to 1.33 sec/km horizontal slowness). Detailed horizontal-slowness measurements using phase correlation shows that there must be two or more modes interfering with each other between 5 and 10 sec arrival time because there are abrupt jumps in phase velocity from one frequency to the next. The fundamental mode Airy phase arrives at 10 sec with a horizontal velocity of about 0.5 km/sec (2.0 sec/km slowness). These attributes of the Rayleigh waves are reflected in the phase-velocity map shown in Figure 7. The method appears to be robust even when a slowly varying wave train of interfering waves is processed. This is empirical evidence that the constraints placed on the variances of the spectral ratios is an appropriate method of analysis to obtain the wave coefficients.

Note that the $A(x)$ coefficient maps for the P wave (Fig. 6) and the Rayleigh wave (Fig. 8), in general, are subdued. Changes occur in the interference between $P_{\text{refracted}}$ and P_{sed} and at the beginning of the Rayleigh wave train. This is consistent with largely plane-wave propagation across the array because of the relatively large distance (2.55 km) of the array from the source and the very slow wave velocities in sediments of the Mississippi embayment.

An Example Using Small-Scale Refraction Data

Gradient analysis may also be useful in analyzing array data collected very near a source where geometrical spreading effects may be large. A common experiment is to collect refraction or reflection data over short distance ranges from

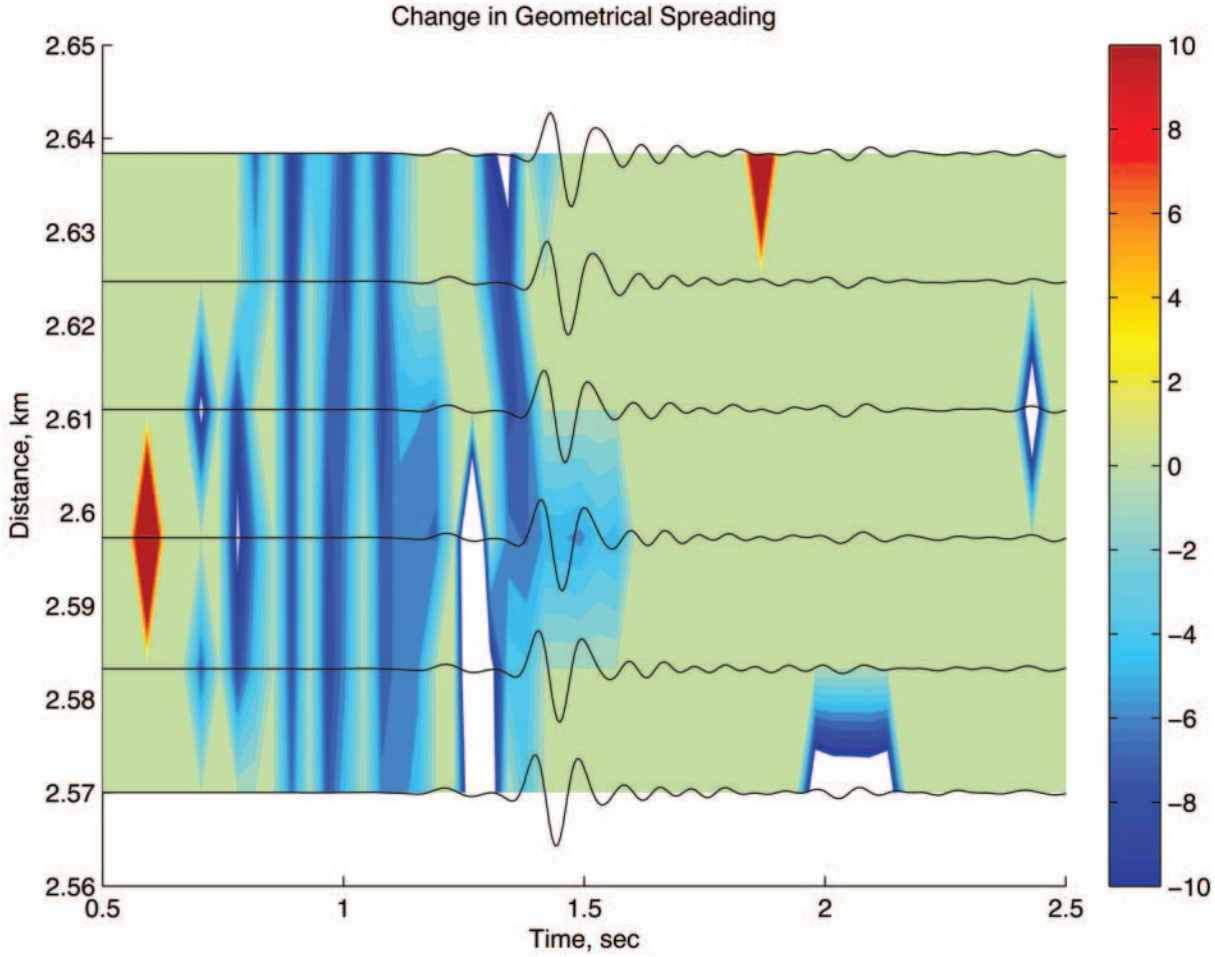

Figure 6. The change in geometrical spreading or the $A(x)$ coefficient plotted as a function of time and space along the array. $A(x)$ is usually close to zero, suggesting the waves are behaving largely as plane waves. Some significant changes occur near 1.25 sec between the two major *P* waves and probably represent interference between the two phases.

the source (~1 to ~100s of meters) with dense linear arrays of instruments. Figure 9 shows a typical data set collected to study near-surface velocity structure for earthquake-hazards evaluation. An *SH*-wave source was situated 2 m from the end of a 24-element geophone spread consisting of horizontal geophones 2 m apart. The data show a refracted *S* wave with a horizontal-phase velocity of 600 m/sec and Love waves with group velocities of 150 m/sec and slower.

Even though the sensor distances are relatively small, it is apparent that these kinds of experiments are spatially aliased with respect to horizontal wavelength because they are designed to observe clear time moveout of seismic phases across the array. Application of the error criterion of equation (32) gives an f_{max} of 9 Hz for waves traveling at 150 m/sec and 37 Hz for waves traveling at 600 m/sec. The Love wave signals in Figure 9 are peaked near 17 Hz and the *S* refraction near 50 Hz, clearly beyond the maximum allowable frequency for accurate spatial derivatives.

The analysis could proceed by low-pass filtering the data to an appropriate frequency band. However, it is expedient to use reducing velocity filtering as presented in equations (19), (20), (21), (22) to first shift the data to a longer apparent horizontal wavelength by reducing the horizontal slowness of phases of interest. Figure 10 shows the result of both time shifting the refraction data by 0.2 sec and then applying a reducing velocity of 160 m/sec to the data to examine Love wave dispersion and amplitude characteristics. Although this degrades the analysis of the *S* refraction by spreading it out in space, the Love wave has been shifted so that small changes in horizontal slowness and its amplitude variations may now be examined using gradient analysis in the dominant frequency band of the Love wave. The effective f_{max} is greater than 200 Hz because the effective horizontal phase velocity is 10 km/sec or higher (from equation 32).

Figures 11 and 12 show the wave-coefficient images for Love waves filtered between 15 and 20 Hz after applying a reducing velocity. There are significant variations in both

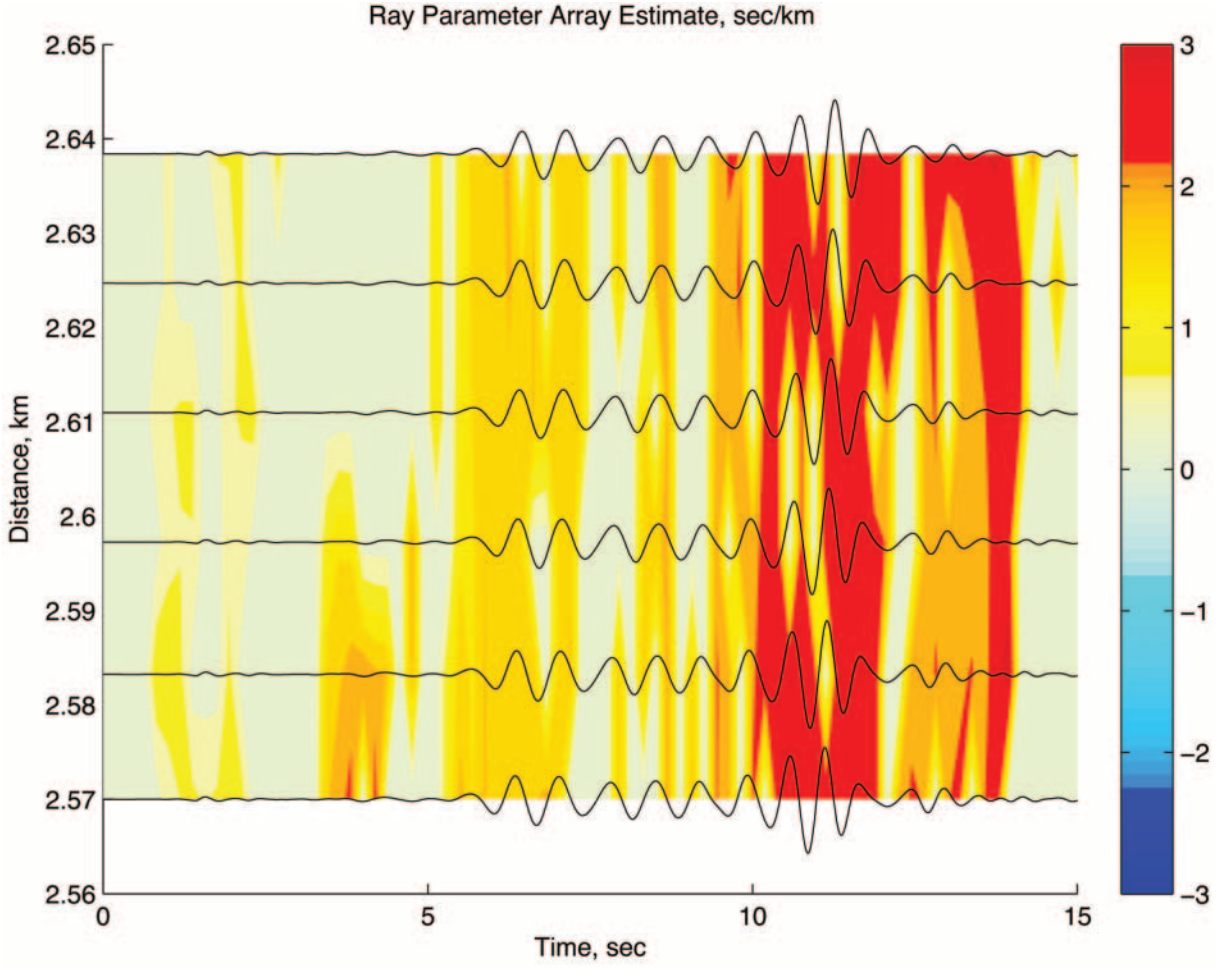

Figure 7. Ray parameter estimate for 1 to 3 Hz vertical Rayleigh waves. The Rayleigh waves start with relatively fast horizontal-phase velocities of about 1 km/sec and end up with slowly propagating Rayleigh waves with velocities near 0.5 km/sec. A 2-sec time window length was assumed in the moving window analysis.

horizontal slowness and relative geometrical spreading for Love waves propagating across the refraction array. Horizontal slowness is negative, in general, indicating that the assumed reducing velocity overcorrected for phase-velocity moveout. However, the yellow areas indicate where Love waves slow down, yielding positive values of relative slowness. The change in geometrical spreading shows its largest variations near the source as expected. However, the Love waves show areas of focusing where the $A(x)$ coefficient actually attains positive values. In general, the Love waves show the effects of wave propagation through heterogeneous media where velocities vary with distance and amplitudes do not obey simple distance power laws.

Discussion

Spatial gradient analysis holds some promise in producing fast estimates of geometrical-spreading changes and horizontal-wave slowness for high-resolution, calibrated, dense seismic arrays. Many array techniques are designed to smooth or average seismic data over the array through correlation and stacking. Taking the spatial gradient of the wave field is diametrically opposite in philosophy since wave differences are employed. "Roughness" of the wave field, if it exists, will be a glaring result. However, it is in this very roughness that a new view of wave propagation in the earth might be obtained. The variation of amplitudes and phase velocities with time along an array represents a highly detailed data set that can be used to understand structural heterogeneity. Roughness can always be smoothed over later in a structure modeling study but represents a truer picture of the actual wave propagation. At a minimum, knowing the variation in amplitudes and phase velocities will aid in a statistical analysis of earth model parameters.

Spatial gradient analysis may be a fast method for producing tomographic images of structure along an array by plotting the anomalies in space and time. As the refraction Love wave example shows, it should be possible collect multiple lines of data over an area and quickly produce a two-dimensional image of phase velocity as a function of fre-

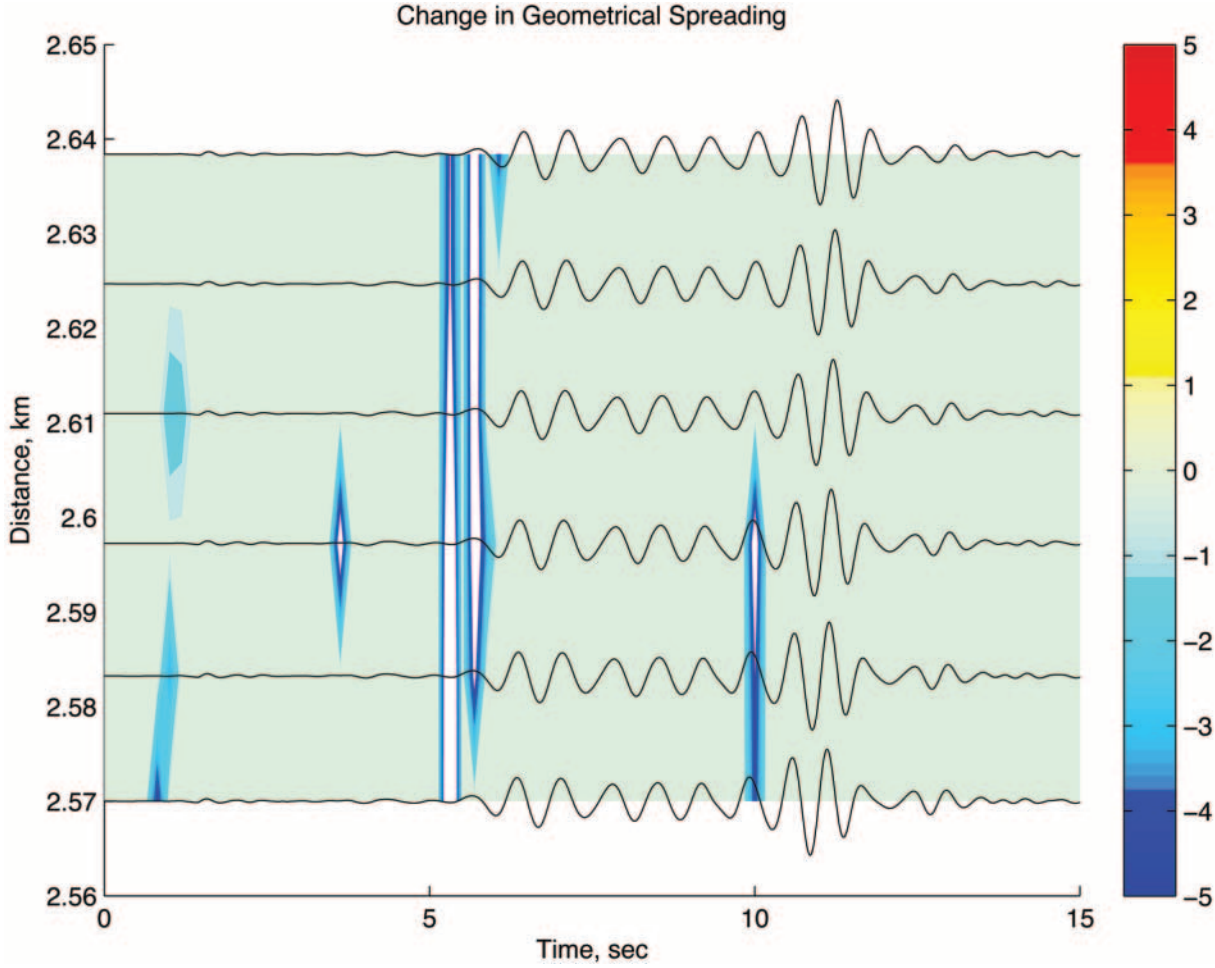

Figure 8. The change in geometrical spreading, or the $A(x)$ coefficient, for the vertical Rayleigh waves. Like the P waves, the Rayleigh waves behave mostly as plane waves. The largest change occurs near the beginning of the Rayleigh arrivals near 5 sec arrival time.

quency. These images might then be used to provide for views of earth structure or analyzed directly to estimate other wave-propagation effects. One use could be in determining near-surface travel-time statics corrections for on-land reflection profiles. Of course, having estimates of ray parameter and amplitude as a function of time is a natural data set for traditional refraction modeling, such as using the venerable Weichert–Herglotz inversion integral.

One of my motivations for examining wave gradients is an attempt to infer the effects of anelasticity or strain-dependent, nonlinear wave propagation in strong ground motion observations. Suppose a wave-gradient analysis is performed after bandpass filtering the data over several frequency bands. Apparent frequency dependence in the geometrical-spreading coefficient, $A(x)$, and the horizontal-wave slowness can be a function of elastic and anelastic wave-propagation effects. Consider the effect of attenuation through a convolutional filter, $f_Q(t, x)$, where the displacement is given by

$$u(t,x) = G(x)f(t - p(x - x_0))*f_Q(t,x). \quad (35)$$

The Fourier transform of equation (35) is

$$\hat{u}(\omega,x) = G(x)\hat{f}(\omega)e^{-i\omega p(x-x_0)}\hat{f}_Q(\omega,x) \quad (36)$$

and the displacement gradient is given by

$$\frac{\partial\hat{u}(\omega,x)}{\partial x} = \hat{D}(\omega,x)\hat{u}(\omega,x), \quad (37)$$

where

$$\hat{D}(\omega,x) = A(x) + i\omega B(x) + \hat{C}(\omega,x) \quad (38)$$

and $A(x)$ and $B(x)$ are given in equations (4) and (5), respectively. The new frequency-dependent coefficient is given by

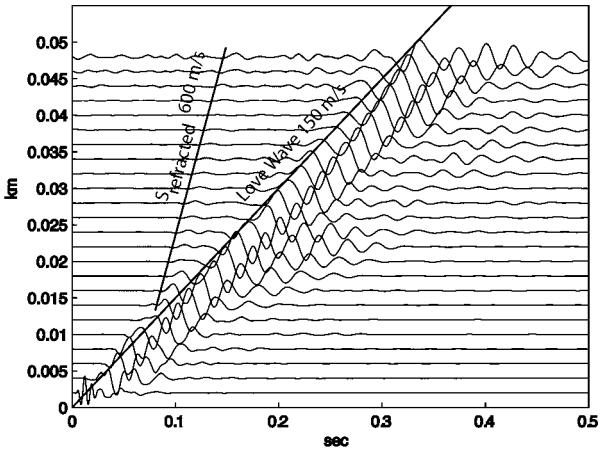

Figure 9. A small scale *SH*-wave refraction data set. The source consists of a horizontal hammer blow on the end of a heavy beam that was pinned to the ground under truck wheels. The source was 2 m from the end of the horizontal geophones and the geophone interval was 2 m. The plot shows Love wave arrivals and an *S*-wave refraction. This kind of data set is spatially aliased as discussed in the text.

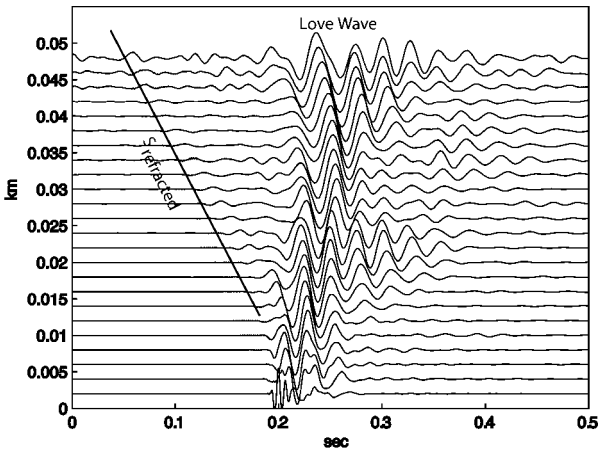

Figure 10. The *SH*-wave refraction data of Figure 9 have been shifted in time by 0.2 sec and a reducing velocity of 150 m/sec applied. A reducing velocity effectively removes the spatial aliasing of the original data because the apparent horizontal velocity becomes quite high.

$$\hat{C}(\omega,x) = \frac{1}{f_Q(\omega,x)}\frac{\partial f_Q(\omega,x)}{\partial x}. \tag{39}$$

For the sake of demonstration, assume a constant horizontal slowness wave with geometrical spreading, such as a surface wave, and a phaseless attenuation operator of the form

$$\hat{f}_Q(\omega,x) = e^{-\gamma(\omega)x}, \tag{40}$$

where γ is the attenuation coefficient. Then,

$$\hat{C}(\omega,x) = -\gamma(\omega) \tag{41}$$

and

$$\hat{D}(\omega,x) = \frac{G'(x)}{G(x)} - i\omega p - \gamma(\omega). \tag{42}$$

Dividing both sides of equation (37) by $\hat{u}(\omega, x)$ and evaluating the real and imaginary parts of (ω, x) gives

$$\frac{G'(x)}{G(x)} - \gamma(\omega) = \mathrm{Re}\left\{\frac{\hat{u}_{,x}(\omega,x)}{\hat{u}(\omega,x)}\right\} \tag{43}$$

and, as before,

$$p = -\frac{1}{\omega}\,\mathrm{Im}\left\{\frac{\hat{u}_{,x}(\omega,x)}{\hat{u}(\omega,x)}\right\}. \tag{44}$$

As in most methods of estimating a spatial attenuation coefficient, finding a value of $\gamma(\omega)$ from equation (43) depends on an assumed form of the geometrical spreading $G(x)$. The attenuation coefficient will be unambiguous for a plane wave ($G(x)$ constant). Alternatively, γ may be known for a particular frequency, ω_0, so that the relative geometrical-spreading change may be estimated by

$$\frac{G'(x)}{G(x)} = \mathrm{Re}\left\{\frac{\hat{u}_{,x}(\omega_0,x)}{\hat{u}(\omega_0,x)}\right\} + \gamma(\omega_0). \tag{45}$$

This allows the use of equation (43) to find $\gamma(\omega)$ at other frequencies. Note that we have not imposed any restrictions on the behavior of γ with frequency, such as being linear or constant. An analysis of geometrical spreading, frequency-dependent geometrical spreading, or finding an attenuation coefficient requires array data over a significant distance range and cannot be performed as a point measurement. Equation (43) demonstrates the usual ambiguity between assigning a distance-amplitude decay to the spreading function or to an effect of anelasticity.

This problem is accentuated when the spectrum of the displacement is highly monochromatic so that it may be impossible to know both the geometrical spreading and the attenuation coefficient as for new field experiments in nonlinear wave propagation (Dimitriu, 1990; Bodin *et al.*, 2004; Pearce *et al.*, 2004). These kinds of experiments employ fixed arrays of strong-motion instruments relative to a strong monochromatic (vibroseis) source to observe changes in wave propagation for changing source strength. Evidence suggests that media velocity decreases and attenuation increases substantially with increasing wave-strain amplitude. In this situation, it should be sufficient to investigate systematic changes in $A(x)$ and $B(x)$ with changes in source strength

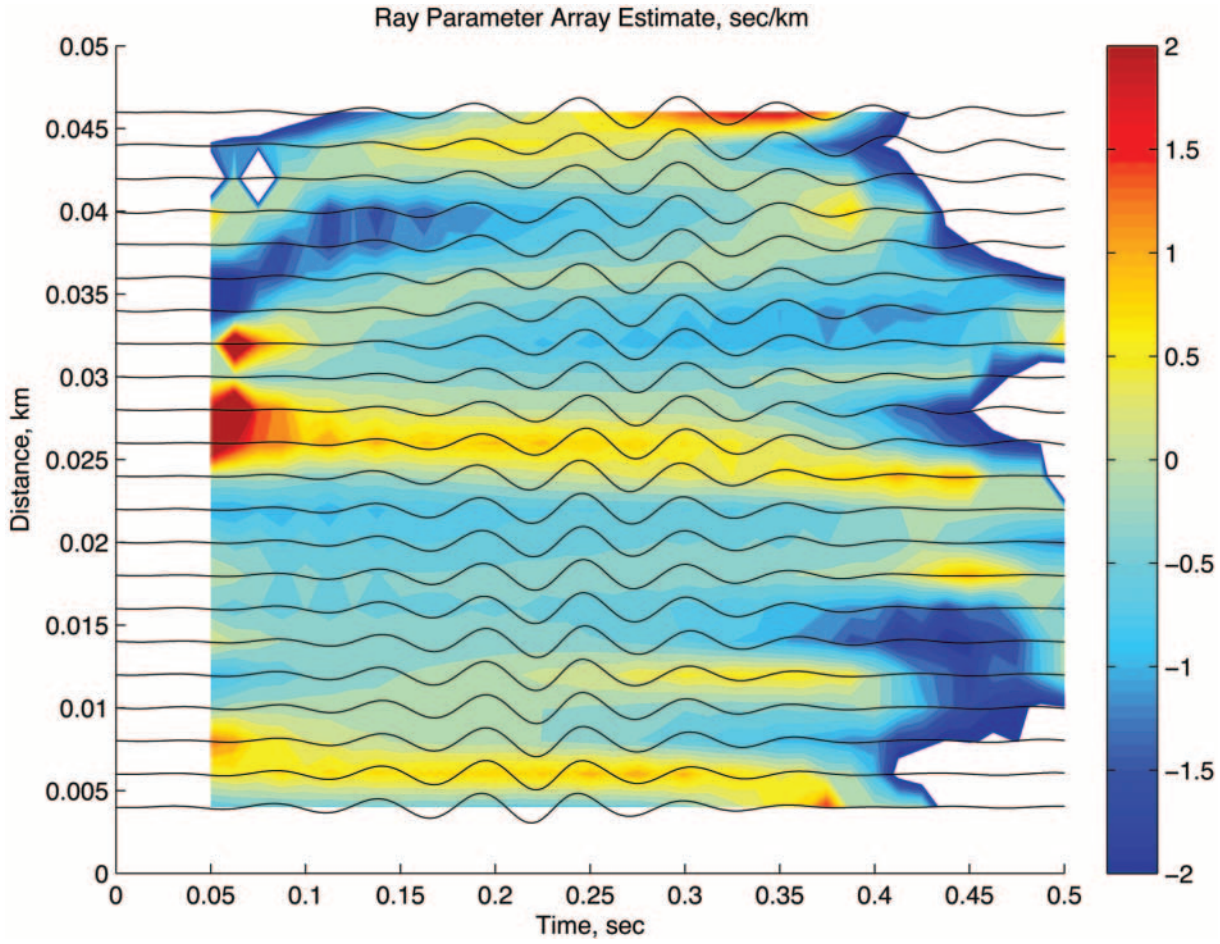

Figure 11. Relative horizontal slowness estimate using spatial gradient analysis. The refraction-profile Love waves have been filtered between 15 and 20 Hz. A reducing velocity of 200 m/sec has also been applied to the original data and a time window length of 0.1 sec was assumed for the moving time window. Values of ray parameter fluctuate across the array as shown by the alternating blue and yellow bands. These fluctuations may to be due to velocity heterogeneity along the array but may also reflect amplitude statics. Horizontal slowness varies from about 4 to 6 sec/km (c = 167 to 250 m/sec) for the Love wave in this frequency band.

by using gradient analysis without an explicit attenuation term to infer effects of material nonlinearity.

The ideas presented in this article are simple and straightforward. They are presented to encourage the use of dense arrays for examining earth structure and the characteristics of nearby seismic sources. In particular, because the spatial gradient is related to strain, these techniques are a natural choice in examining strain-dependent wave propagation in strong ground motions from earthquakes and controlled sources. Near-surface soils undergo strain-dependent modulus degradation under strong ground motions (e.g., Bolton *et al.*, 1986; Vucetic, 1994). These effects are important in evaluating the hazards from strong ground motions in large earthquakes. Using spatial gradient analysis for dense strong-motion arrays may be a viable way to test *in situ* soil nonlinearity by observing changes in both effective geometrical spreading and horizontal-phase velocities with increasing strain amplitude (Bodin *et al.*, 2004).

Acknowledgments

This work was supported by the Mid America Earthquake Center through contract HD-3 and HD-5. Ting-Li Lin helped collect the *SH*-wave refraction data used in this article and is gratefully acknowledged. Joan Gomberg read the first draft of this manuscript and made many useful suggestions. The manuscript was also improved by comments made by two anonymous reviewers. This is CERI contribution no. 503.

References

Abrahamson, N. A. (1991). Empirical spatial coherency functions for application to soil-structure interaction analyses, *Earthquake Spectra* **7,** 1–28.

Abramowitz, M., and I. A. Stegun (1968). *Handbook of Mathematical Functions*, Dover Publications, New York.

Agnew, D. C. (1986). Strainmeters and tiltmeters, *Rev. Geophys.* **24,** 579–624.

Bodin, P., T. Brackman, Z. Lawrence, J. Gomberg, J. Steidl, F. Meng, K. Stokoe, P. Johnson, and F. Pearce (2004). Monitoring non-linear wave

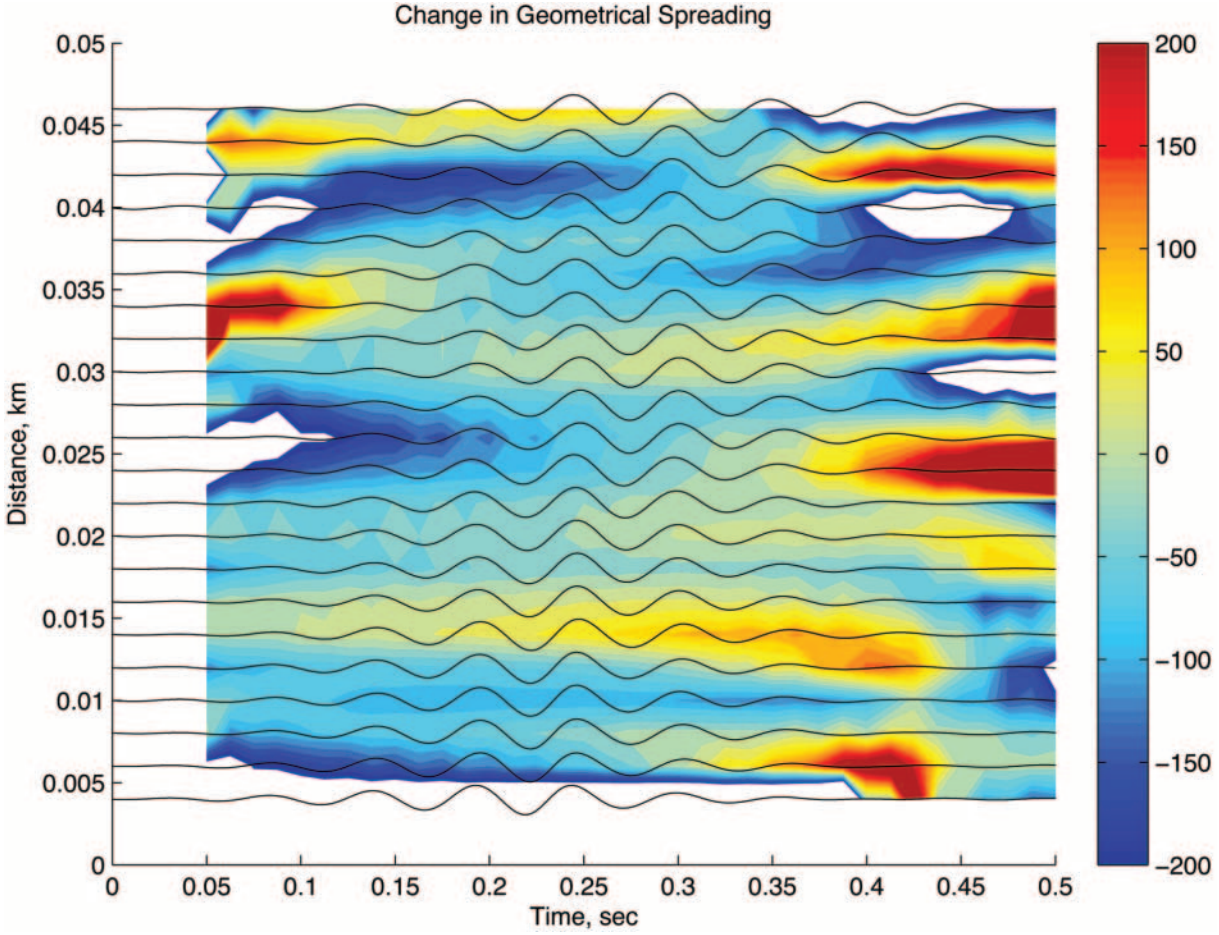

Figure 12. The change in geometrical spreading, or the $A(x)$ coefficient, for the filtered Love wave data. There is a large change in geometrical spreading near the source, as expected, but the relative change has both negative and positive values along the array. Ideally, the $A(x)$ coefficient should be negative and tend toward zero with distance.

propagation in the 2004 Garner Valley demonstration project, *EOS Trans. AGU* **85,** S43 A-0975.

Bodin, P., J. Gomberg, S. K. Singh, and M. Santoyo (1997). Dynamic deformations of shallow sediments in the Valley of Mexico, part I: Three-dimensional strains and rotations recorded on a seismic array, *Bull. Seism. Soc. Am.* **87,** 528–539.

Bolton, H., R. T. Wong, I. M. Idriss, and K. Tokmatsu (1986). Moduli and damping factors for dynamic analysis of cohesionless soils, *J. Tech. Eng.* **112,** 1016–1032.

Bungum, H., E. S. Huseby, and F. Ringdal (1971). The NORSAR array and preliminary results of data analysis, *Geophys. J. R. Astr. Soc.* **25,** 115–126.

Cranswick, E., R. Wetmiller, and J. Boatwright (1985). High-frequency observations and source parameters of microearthquakes recorded at hard-rock sites, *Bull. Seism. Soc. Am.* **75,** 1535–1567.

Dimitriu, P. P. (1990). Preliminary results of vibrator-aided experiments in non-linear seismology conducted at Uetze, F.R.G., *Phys. Earth Planet. Interiors* **63,** 172–180.

Gershenfeld, N. (1999). *The Nature of Mathematical Modeling*, Cambridge University Press, Cambridge, 344 pp.

Gomberg, J., and D. Agnew (1996). The accuracy of seismic estimates of dynamic strains: an evaluation using strainmeter and seismometer data from Pinon Flat Observatory, California, *Bull. Seism. Soc. Am.* **86,** 212–220.

Gomberg, J., G. Pavlis, and P. Bodin (1999). The strain in the array is mainly in the plane (waves below ~1 Hz), *Bull. Seism. Soc. Am.* **89,** 1428–1438.

Gomberg, J. S., P. A. Bodin, and V. Martinov (1988). Seismic system calibration using cross-spectral methods from in situ measurements: the Kazakh, USSR, Phase I array, *Bull. Seism. Soc. Am.* **78,** 1380–1386.

Harichandran, R. S., and E. H. Vanmarcke (1986). Stochastic variation of earthquake ground motion in space and time, *J. Eng. Mech. ASCE* **112,** 154–174.

Langston, C. A. (2007). Wave gradiometry in two dimensions, *Bull. Seism. Soc. Am.* (in press).

Langston, C. A., P. Bodin, C. Powell, M. Withers, S. Horton, and W. Mooney (2006). Explosion source strong ground motions in the Mississippi embayment, *Bull. Seism. Soc. Am.* **96,** 1038–1054.

Lomnitz, C. (1997). Frequency response of a strainmenter, *Bull. Seism. Soc. Am.* **87,** 1078–1080.

Pearce, F., P. Bodin, T. Brackman, Z. Lawrence, J. Gomberg, J. Steidl, F. Meng, R. Guyer, K. Stokoe, and P. A. Johnson (2004). Nonlinear soil response induced in situ by an active source a Garner Valley, *EOS Trans. AGU* **85,** S42A-04.

Spudich, P., L. K. Steck, M. Hellweg, J. B. Fletcher, and L. M. Baker (1995). Transient stresses at Parkfield, California, produced by the M7.4 Landers earthquake of June 28, 1992: observations from the UPSAR dense seismograph array, *J. Geophys. Res.* **100,** 675–690.

Vucetic, M. (1994). Cyclic threshold shear strains in soils, *J. Geotech. Eng.* **120,** 2208–2228.

Whitham, G. B. (1999). *Linear and Nonlinear Waves*, John Wiley & Sons, Inc., New York.

Zerva, A., and V. Zervas (2002). Spatial variation of seismic ground motions: an overview, *Appl. Mech. Rev.* **55,** 271–297.

Appendix

Computation of the Displacemnet Gradient

The crux of this technique lies in being able to accurately obtain the displacement gradient. Seismological observations almost always consist of high-quality point measurements of filtered ground displacement, velocity, or acceleration. Few instruments directly record strain or differential displacement outside of instrumentation located at special observatories (Agnew, 1986; Gomberg and Agnew, 1996). Based on the success of past array studies for estimating the displacement gradient and strain (e.g., Spudich *et al.*, 1995; Bodin *et al.*, 1997; Gomberg *et al.*, 1999; Langston *et al.*, 2006), I take the approach of using finite differences between separate seismometers to compute the displacement gradient. It is instructive to look at this computation in some detail since there are several sources of error that will occur because of experiment design, instrumentation calibration, seismometer installation, and amplitude and phase "statics" problems from real earth structure.

Consider a linear array of n seismometers with spacing Δx. Because we want to compare the displacement gradient, displacement, and velocity all at the same location, it is appropriate to use the mean of the forward and backward difference at each seismometer location, excluding the endpoint locations. This estimate of the displacement derivative has second-order accuracy in the distance increment (Abramowitz and Stegun, 1968; Gershenfeld, 1999). Explicitly and keeping the error term,

$$\left.\frac{\partial u}{\partial x}\right|_x = \frac{u(t, x + \Delta x) - u(t, x - \Delta x)}{2\Delta x} - \frac{1}{6}\left.\frac{\partial^3 u}{\partial x^3}\right|_x \Delta x^2. \quad \text{(A1)}$$

The error due to sampling for a sinusoidal wave can be estimated by assuming a plane wave of the form

$$u(t, x) = e^{i\omega(t - px)}. \quad \text{(A2)}$$

Requiring that the error in the first derivative be less than some threshold, δ, gives

$$\left| \frac{-\frac{1}{6}\left.\frac{\partial^3 u}{\partial x^3}\right|_x \Delta x^2}{\left.\frac{\partial x}{\partial u}\right|_x} \right| = \frac{1}{6}\omega^2 p^2 \Delta x^2 \le \delta. \quad \text{(A3)}$$

Since

$$k = \omega p = \frac{2\pi}{\lambda}, \quad \text{(A4)}$$

where λ is the horizontal wavelength and k is the horizontal wavenumber. For $\delta = 0.1$ (10% error), the sampling interval must be

$$\Delta x \le \lambda \frac{\sqrt{1.5\delta}}{\pi} = 0.123\lambda. \quad \text{(A5)}$$

In other words, the sampling interval must be about 12% of the horizontal wavelength to attain an accuracy of 10% in the spatial derivative. Equation (A3) is useful for estimating the maximum wavenumber that is resolvable for a particular array using this finite-difference operator.

Center for Earthquake Research and Information
University of Memphis
3876 Central Ave., Suite 1
Memphis, Tennessee 38152-3050

Manuscript received 4 May 2006.